Performance Analysis And Optimization Of The Cdif Coal-Fired Generator

Author(s): V. W. Daniel

Session Name: Generators B

SEAM: 28 (1990)

SEAM EDX URL: https://edx.netl.doe.gov/dataset/seam-28

EDX Paper ID: 1431

PERFORMANCE ANALYSIS AND OPTIMIZATION OF THE CDIF COAL-FIRED GENERATOR

Victor W. Daniel
Staff Scientist
MSE, Inc.
Butte, Montana 59702

ABSTRACT

A simple, one-dimensional, electrical model is developed for linear magnetohydrodynamic (MHD) generators and is used to analyze the performance of the Component Development and Integration Facility (CDIF) generator. This simple MHD model is applicable to Faraday and diagonal operation modes. Starting with suitably averaged Ohm's law relations and Maxwell's equations, a closed-form solution is obtained for the basic MHD equations. The key to this development is the introduction of a net nonuniformity factor that accounts for transverse nonuniformities through the plasma and slag layers. With this approach, separate transverse voltage drop and axial leakage terms are not needed since the net nonuniformity factor properly accounts for both of these losses. For both modes of operation, simple lumped-circuit models are developed as aids in understanding the basic principles involved in MHD power generation. From the basic MHD equations, new methods are developed for computing important channel properties in terms of routine experimental data and good estimates for the average plasma velocity and Hall parameter. Simple experiments are described to accurately measure the average plasma velocity and average Hall parameter at any axial location. Among the channel properties that can be estimated using these methods are the slag axial leakage current, the plasma axial current, the channel axial resistance per pitch, the channel transverse resistance per pitch, the net nonuniformity factor, the local load factor, and the optimal diagonal link overlap--all under power generation conditions. Using the closed-form solutions, several CDIF tests are analyzed in detail, and optimal link configurations are computed for maximum power production. From this analysis, serious deficiencies are identified in the CDIF generator as it is presently configured, particularly for diagonal connections. Specifically, it is shown that the presence of coal slag has forced the CDIF generator to operate off-design. Recommendations are given to improve generator performance for more power at less stress. In addition, it is shown that Faraday and diagonal modes should produce the same local power densities (and hence total power) when both modes are optimally configured and loaded for maximum power extraction.

INTRODUCTION

Over the past decade, several simple magnetohydrodynamic (MHD) models have appeared in the MHD literature and elsewhere. Although these models adequately explain many important MHD phenomena, they all ignore significant effects caused by plasma/slag nonuniformities. However, it is difficult to include all significant effects in any simple, one-dimensional model. The one-dimensional model originally proposed by Wu[1] and later updated by Nelson et al.[2] handles transverse nonuniformities via a nondimensional voltage drop and handles axial slag leakage via an imposed axial current. A variant of this model proposed by Pian et al.[3] handles axial slag leakage via an axial slag resistance per pitch. However, both of these models assume a uniform plasma (nonuniformity factor $G = 1$) and dump all plasma nonuniformity effects onto the transverse voltage drop and axial leakage terms. Another interesting model proposed by Solbes[4] handles plasma nonuniformities but ignores wall leakage effects. Recent studies by Daniel[5] and Nelson[2], however, indicate that slag leakage currents can be quite large (often over 100 A) for the Component Development and Integration Facility (CDIF) channel and cannot be ignored.

This paper proposes a simple, one-dimensional model based on a net nonuniformity factor to account for plasma/slag transverse nonuniformities. Since these transverse nonuniformities are primarily responsible for the large axial currents believed to exist in coal-fired MHD generators, this model should represent a significant advancement over previous one-dimensional models in terms of accuracy and simplicity (explicit transverse voltage drop and axial leakage terms are not needed in the model). Plasma transverse nonuniformities are automatically included in the model; however, axial nonuniformities and transverse leakage currents are generally ignored.

SIMPLIFYING ASSUMPTIONS

Closed-form solutions will be obtained for linear MHD channels of the type shown in Figure 1. Although the channel walls illustrated in Figure 1 are straight, this does not have to be the case in the general treatment that follows. The standard right-handed coordinate system commonly used in the MHD community is adopted for this development and is shown in Figure 1. To reduce the complexity of the MHD problem, the following simplifying assumptions are needed:

- generator is operated in a steady-state condition,
- changes in z direction are negligible,
- E_x and J_y are constant on any cross section, and
- plasma changes due to channel loading are negligible.

Basically, these assumptions apply to low-interaction MHD channels in which transient effects and sidewall effects are negligible.

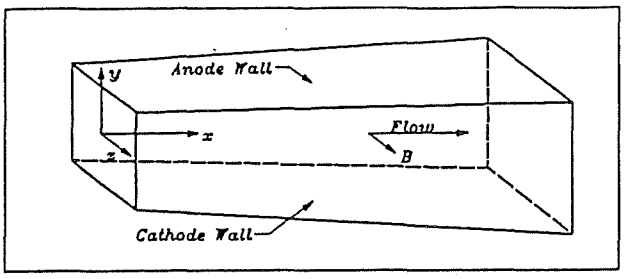

FIGURE 1 — LINEAR MHD CHANNEL

Fundamental to this development is the introduction of the cross-sectional average operator $\langle\cdot\rangle$ defined by

$$\langle q\rangle = \frac{1}{A}\int_A q\,dA \tag{1}$$

for any quantity q. The averaging in equation (1) is over the entire channel cross section A, including the slag layers. Operator $\langle\cdot\rangle$ is linear since

$$\langle q_1 + q_2\rangle = \langle q_1\rangle + \langle q_2\rangle \tag{2}$$

$$\langle cq\rangle = c\langle q\rangle \tag{3}$$

where c is any constant quantity (over cross section A). It follows from the simplifying assumptions that the Faraday voltage V_f and the net axial current I_x can be expressed in terms of the cross-sectional averages of E_y and J_x as follows:

$$V_f = H\langle E_y\rangle \tag{4}$$

$$I_x = A\langle J_x\rangle \tag{5}$$

where H is the channel height.

OHM'S LAW RELATIONS

The basic constitutive relation that connects the current density J, the electric field E, the plasma velocity U, and the magnetic flux B is Ohm's law, which in vector form is

$$\mathbf{J} + \mu\mathbf{J}\times\mathbf{B} = \sigma(\mathbf{E} + \mathbf{U}\times\mathbf{B}) \tag{6}$$

where μ is the electron mobility and σ is the conductivity of the medium (plasma or slag). In the slag layers, one can assume μ to be zero for all practical purposes. In MHD plasmas, however, μ can be relatively large and the J×B term gives rise to a substantial Hall field whose effects can not be ignored. Assuming the z components are negligible, as well as the transverse velocity component, Ohm's law can be expressed in component form as follows:

$$E_x = \frac{1}{\sigma}(J_x + \beta J_y) \tag{7}$$

$$E_y = \frac{1}{\sigma}(J_y - \beta J_x) + uB \tag{8}$$

$$J_x = \frac{\sigma}{1+\beta^2}(E_x - \beta E_y + \beta uB) \tag{9}$$

$$J_y = \frac{\sigma}{1+\beta^2}(E_y + \beta E_x - uB) \tag{10}$$

where $\beta = \mu|B|$ is the Hall parameter.

Equations (7) through (10) are essentially three-dimensional in nature but can be reduced to one-dimensional form by an averaging technique originally developed by Rosa.[6] The key to this development is to average the two Ohm's law equations that contain only one J_x or E_y term but not both terms. Following Rosa's methods, one eventually obtains the averaged Ohm's law equations:

$$E_x = \frac{1}{\langle\sigma\rangle}[\langle J_x\rangle + \langle\beta\rangle J_y] \tag{11}$$

$$\langle E_y\rangle = \frac{1}{\langle\sigma\rangle}[GJ_y - \langle\beta\rangle\langle J_x\rangle] + \langle uB\rangle \tag{12}$$

$$\langle J_x\rangle = \frac{\langle\sigma\rangle}{G + \langle\beta\rangle^2}[GE_x - \langle\beta\rangle\langle E_y\rangle + \langle\beta\rangle\langle uB\rangle] \tag{13}$$

$$J_y = \frac{\langle\sigma\rangle}{G + \langle\beta\rangle^2}[\langle E_y\rangle + \langle\beta\rangle E_x - \langle uB\rangle] \tag{14}$$

where

$$G = \langle\sigma\rangle\left\langle\frac{1+\beta^2}{\sigma}\right\rangle - \langle\beta\rangle^2 \tag{15}$$

is the net nonuniformity factor (Rosa G factor). It is shown in reference 7 that $G \geq 1$ always holds with equality holding if and only if both σ and β are constant on cross section A. The one-dimensional (averaged) equations (11) through (14) are surprisingly similar to the original three-dimensional equations (7) through (10). The only difference, other than the appearance of average values everywhere, is the occasional insertion of a nonuniformity factor G in these formulas. The averaged Ohm's law equations are redundant since any two of them will suffice (the remaining equations can be easily derived from the selected pair of equations).

BASIC MHD EQUATIONS

To obtain a closed-form solution for the four electrodynamic variables E_x, $\langle E_y\rangle$, $\langle J_x\rangle$, and J_y in terms of the gas dynamic variables and the channel configuration, it is necessary to find four independent equations relating these four quantities. The averaged Ohm's law equations provide two of the needed equations. The remaining two equations are derived from Maxwell's equations and contain the boundary conditions.

The first Maxwell equation needed is Faraday's law, which in light of the simplifying assumptions can be expressed in integral form as follows:

$$\int_C E\cdot dl = 0 \tag{16}$$

where C is any closed curve. Choosing loop C to be the right triangle formed by the diagonal link as shown in Figure 2, one obtains

$$V_f = I_b R_b + nV_h$$
$$-A_e J_y R_b = npE_x + H\langle E_y\rangle$$
$$-r_b J_y = \langle\sigma\rangle[lE_x + \langle E_y\rangle] \tag{17}$$

where n is the link overlap, p is the electrode pitch, A_e is the electrode (plus insulator) surface area, I_b

is the link current, R_b is the ballast resistance, V_A is the Hall voltage per pitch, θ is the link overlap angle, and

$$t = \tan\theta = \frac{np}{H} \tag{18}$$

$$r_b = \frac{\langle\sigma\rangle A_c}{H} R_b \tag{19}$$

quantity t is the link overlap parameter and r_b is the nondimensional ballast resistance.

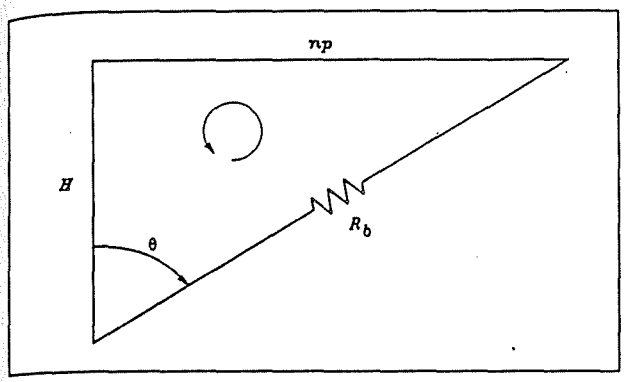

FIGURE 2 — CLOSED LOOP C

The second Maxwell equation needed is the continuity of current law, which in light of the simplifying assumptions can be expressed in integral form as follows:

$$\int_S J \cdot dS = 0 \tag{20}$$

where S is any closed surface. Choosing S to be the infinite plane (closed at infinity) perpendicular to the channel axis as shown in Figure 3, one obtains

$$\begin{aligned} I &= I_x + nI_y \\ &= A\langle J_x\rangle - nA_c J_y \\ &= A[\langle J_x\rangle - tJ_y] \end{aligned} \tag{21}$$

where I is the load current and I_y is the transverse current per pitch (assumed to be the same as I_b).

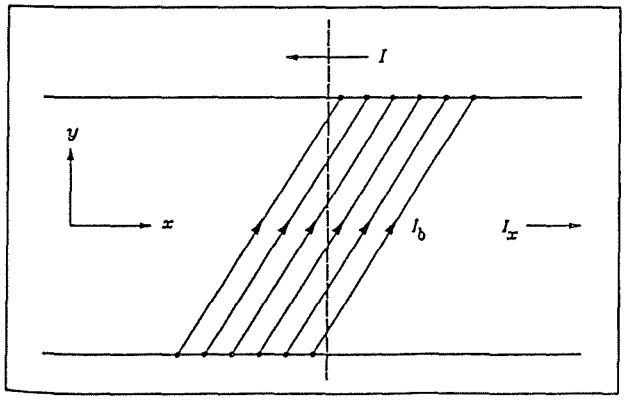

FIGURE 3 — CLOSED SURFACE S (INDICATED BY DOTTED LINE)

Choosing the first and last of the averaged Ohm's law equations and the two Maxwell equations, the complete set of MHD equations become

$$\langle J_x\rangle = \langle\sigma\rangle E_x - \langle\beta\rangle J_y \tag{22}$$

$$\langle E_y\rangle = -\langle\beta\rangle E_x + \frac{G + \langle\beta\rangle^2}{\langle\sigma\rangle} J_y + \langle uB\rangle \tag{23}$$

$$-r_b J_y = \langle\sigma\rangle[tE_x + \langle E_y\rangle] \tag{24}$$

$$I = A[\langle J_x\rangle - tJ_y] \tag{25}$$

Solving these four independent equations for E_x, $\langle E_y\rangle$, $\langle J_x\rangle$, and J_y in terms of the channel configuration and gas dynamic properties, one obtains

$$E_x = \frac{(G + \langle\beta\rangle^2 + r_b)I - \langle\sigma\rangle A(\langle\beta\rangle + t)\langle uB\rangle}{\langle\sigma\rangle A(G + t^2 + r_b)} \tag{26}$$

$$\langle E_y\rangle = \frac{-(Gt + t\langle\beta\rangle^2 + \langle\beta\rangle r_b)I + \langle\sigma\rangle A(t\langle\beta\rangle + t^2 + r_b)\langle uB\rangle}{\langle\sigma\rangle A(G + t^2 + r_b)} \tag{27}$$

$$\langle J_x\rangle = \frac{(G + t\langle\beta\rangle + r_b)I - \langle\sigma\rangle At\langle uB\rangle}{A(G + t^2 + r_b)} \tag{28}$$

$$J_y = \frac{(\langle\beta\rangle - t)I - \langle\sigma\rangle A\langle uB\rangle}{A(G + t^2 + r_b)} \tag{29}$$

In view of the simplifying assumptions, these one-dimensional equations yield only the average values of the electrodynamic variables at each axial location.

GLOBAL HALL SOLUTION

The global Hall solution can be obtained from the local solution by integrating equation (26) over the channel length:

$$\begin{aligned} V &= -\int_0^L E_x dx \\ &= -\left[\int_0^L \frac{(\langle\beta\rangle + t)\langle uB\rangle}{G + t^2 + r_b} dx\right] - \left[\int_0^L \frac{G + \langle\beta\rangle^2 + r_b}{G + t^2 + r_b} \frac{dx}{\langle\sigma\rangle A}\right] I \end{aligned} \tag{30}$$

The bracketed expressions above can be assumed constant over a load sweep since experimental load lines for the CDIF channel are nearly linear. Thus, equation (30) reduces to

$$V = V_{oc} - IR^* \tag{31}$$

where V_{oc} is the open circuit voltage given by

$$V_{oc} = \int_0^L \frac{(\langle\beta\rangle + t)\langle uB\rangle}{G + t^2 + r_b} dx \tag{32}$$

and R^* is the generator internal resistance given by

$$R^* = \int_0^L \frac{G + \langle\beta\rangle^2 + r_b}{G + t^2 + r_b} \frac{dx}{\langle\sigma\rangle A} \tag{33}$$

The short circuit current I_{sc} is obtained by setting $V = 0$ in equation (31):

$$I_{sc} = \frac{V_{oc}}{R^*} \tag{34}$$

In practice, V_{oc} and I_{sc} are obtained from load line extrapolations as shown in Figure 4, and R^* is

computed from equation (34) or directly from the slope of the experimental load line.

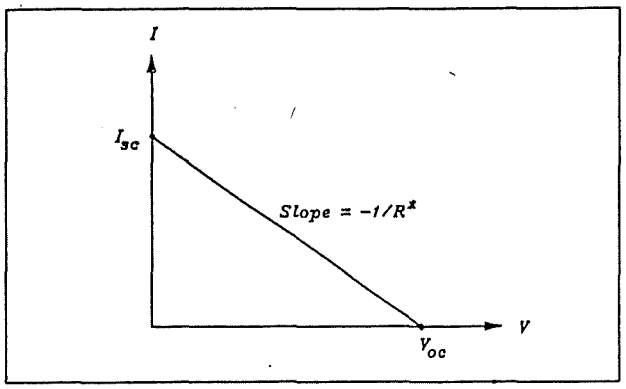

FIGURE 4 — GLOBAL HALL LOAD LINE

Internal resistance R° is not the same as the bulk resistance R' that is normally measured by applying a voltage along the channel length with the magnetic field turned off and the external links disconnected. The bulk resistance R' is given by

$$R' = \int_0^L \frac{dx}{\langle\sigma\rangle A} \tag{35}$$

Both R° and R' are sensitive to slag shorting via the $\langle\sigma\rangle$ term, with both resistances tending to decrease as polarization develops.

The Hall voltage V is related to the load current I and load resistance R via the lumped circuit Ohm's law:

$$V = IR \tag{36}$$

From equations (31) and (36), it follows that the open circuit voltage is given by

$$V_{oc} = IR + IR^\circ = I(R + R^\circ) \tag{37}$$

Consequently, a global load factor K can be defined by

$$K = \frac{V}{V_{oc}} = \frac{R}{R + R^\circ} \tag{38}$$

From equations (31), (34), (36), and (38), it follows that

$$V = KV_{oc} \tag{39}$$

$$I = \frac{V_{oc} - V}{R^\circ} = \frac{V_{oc} - KV_{oc}}{R^\circ} = (1-K)I_{sc} \tag{40}$$

$$R = \frac{V}{I} = \frac{KV_{oc}}{(1-K)I_{sc}} = \frac{K}{1-K}R^\circ \tag{41}$$

$$P_h = VI = K(1-K)V_{oc}I_{sc} \tag{42}$$

where P_h is the Hall power extracted. Clearly, P_h is maximal when $K = 1/2$ or, equivalently, $V = (1/2)V_{oc}$, $I = (1/2)I_{sc}$, or $R = R^\circ$. However, total power $P = P_h + P_b$ is not necessarily maximal at this condition.

POWER RELATIONS

Using the simplifying assumptions, the electrical power, mechanical power, and Joule heating power loss can be easily expressed in terms of measured voltages and currents and the average (motional) electromotive force $\langle uB\rangle$. The electrical power extracted per pitch is given by

$$\begin{aligned}\Delta P &= -pA\langle \mathbf{J}\cdot\mathbf{E}\rangle \\ &= -pA(\langle J_x\rangle E_x + J_y\langle E_y\rangle) \\ &= I_x V_h + I_y V_l\end{aligned} \tag{43}$$

Using relations (17) and (21), equation (43) can be recast into the following alternate form:

$$\begin{aligned}\Delta P &= IV_h + I_b^2 R_b \\ &= \Delta P_h + \Delta P_b\end{aligned} \tag{44}$$

where $\Delta P_h = IV_h$ and $\Delta P_b = I_b^2 R_b$ are the Hall power and ballast power extracted per pitch, respectively.

The plasma, as it moves down the channel, gives up some of its energy to generate electric power externally and Joule heating internally. This net power extracted from the plasma is usually called the mechanical power and is denoted by P_M. The mechanical power extracted per pitch is given by

$$\begin{aligned}\Delta P_M &= pA\langle \mathbf{J}\cdot\mathbf{U}\times\mathbf{B}\rangle \\ &= -HA_c J_y\langle uB\rangle \\ &= I_y\langle uB\rangle H\end{aligned} \tag{45}$$

From equations (6), (43), and (45), one obtains the Joule heating power loss per pitch ΔP_J as follows:

$$\begin{aligned}\Delta P_J &= pA\langle |\mathbf{J}|^2/\sigma\rangle \\ &= \Delta P_M - \Delta P \\ &= -I_x V_h + I_y(\langle uB\rangle H - V_l)\end{aligned} \tag{46}$$

The three power quantities can also be expressed in terms of the channel configuration and gas dynamic properties. Starting with the local solution equations (26) through (29), one eventually obtains:

$$\Delta P = \frac{p}{\langle\sigma\rangle A}\frac{r_b\langle\sigma\rangle^2 A^2\langle uB\rangle^2 + Q_1\langle\sigma\rangle A\langle uB\rangle I - Q_2 I^2}{(G + t^2 + r_b)^2} \tag{47}$$

$$\Delta P_M = \frac{p}{\langle\sigma\rangle A}\frac{\langle\sigma\rangle^2 A^2\langle uB\rangle^2 - (\langle\beta\rangle - t)\langle\sigma\rangle A\langle uB\rangle I}{G + t^2 + r_b} \tag{48}$$

$$\Delta P_J = \frac{p}{\langle\sigma\rangle A}\frac{(G + t^2)\langle\sigma\rangle^2 A^2\langle uB\rangle^2 - Q_3\langle\sigma\rangle A\langle uB\rangle I + Q_2 I^2}{(G + t^2 + r_b)^2} \tag{49}$$

where

$$Q_1 = (\langle\beta\rangle + t)(G + t^2) + (3t - \langle\beta\rangle)r_b \tag{50}$$

$$Q_2 = (G + \langle\beta\rangle^2)(G + t^2) + (2G + 2t\langle\beta\rangle + r_b)r_b \tag{51}$$

$$Q_3 = 2\langle\beta\rangle(G + t^2) + 2tr_b \tag{52}$$

LUMPED CIRCUIT MODELS

The axial lumped circuit model for one pitch can be derived from equation (11) as follows:

$$-pE_x = -\frac{\langle\beta\rangle}{\langle\sigma\rangle W} A_s J_y - \frac{p}{\langle\sigma\rangle A} A \langle J_x \rangle$$

$$V_h = V_x - I_x R_x \tag{53}$$

where W is the channel width and

$$V_x = \frac{\langle\beta\rangle}{\langle\sigma\rangle W} I_y \tag{54}$$

$$R_x = \frac{p}{\langle\sigma\rangle A} \tag{55}$$

Voltage V_x is an axial voltage source induced by the transverse current I_y and R_x is the channel axial resistance per pitch. Resistance R_x is related to the total bulk resistance R' as follows:

$$R' = \Sigma \Delta R' = \Sigma R_x \tag{56}$$

Consequently, it is sometimes convenient to denote R_x by $\Delta R'$. For similar reasons, the (per pitch) Hall voltage V_h will sometimes be denoted by ΔV.

The transverse lumped circuit model for one pitch can be derived from equation (12) as follows:

$$H \langle E_y \rangle = \langle uB \rangle H - \frac{\langle\beta\rangle A}{\langle\sigma\rangle W} \langle J_x \rangle + \frac{GHA_s}{\langle\sigma\rangle A_s} J_y$$

$$V_l = \langle uB \rangle H - V_y - I_y R_y \tag{57}$$

where

$$V_y = \frac{\langle\beta\rangle}{\langle\sigma\rangle W} I_x \tag{58}$$

$$R_y = \frac{GH}{\langle\sigma\rangle A_s} \tag{59}$$

Voltage V_y is a transverse voltage drop induced by the net axial current I_x if I_x is positive, otherwise V_y becomes a voltage source. Resistance R_y is the transverse resistance per pitch across the channel and includes the slag layer contribution.

The axial and transverse lumped circuit models are coupled via the V_x and V_y voltages, which in turn are proportional to I_y and I_x, respectively. These lumped circuit models may be joined as indicated in Figure 5 to obtain a local lumped circuit model for one pitch. When the local lumped circuits are connected with the appropriate external links as shown in Figure 6, a global lumped circuit network results. Unless the generator is operated in a current control mode, the lumped circuit elements in the global network are coupled via the load current I, with local plasma/slag conditions being felt throughout the channel through their influence on the load current. However, when the generator is operated in current control mode, which includes Faraday operation, it follows from equations (26) through (29) that the local steady-state solution depends only on the local plasma/slag conditions.

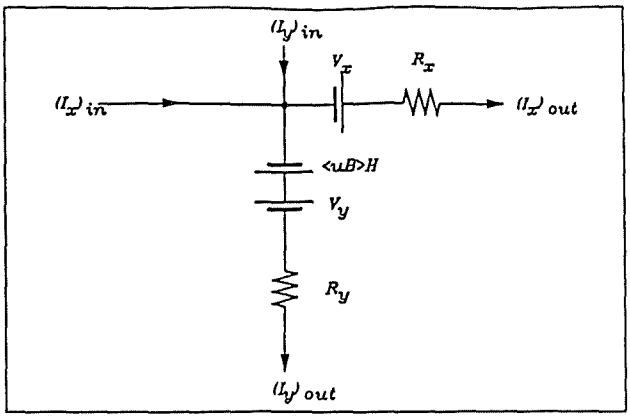

FIGURE 5 — LOCAL LUMPED CIRCUIT MODEL

The coupling between the axial and transverse lumped circuits can be fairly strong. From equations (54) and (58), it follows immediately that

$$V_x I_x = V_y I_y \tag{60}$$

That is, the power source in the axial circuit is exactly equal to the power sink in the transverse circuit (ignoring Joule heating losses). Hence, power is being shuffled from the transverse circuit to the axial circuit if I_x is positive; otherwise, the direction of power flow is reversed. From equations (46), (53), (57), and (60), it follows that the Joule heating power loss per pitch is given by

$$\Delta P_J = I_x^2 R_x + I_y^2 R_y \tag{61}$$

as expected. It is clear from this equation that channel performance is highly dependent on the values of R_x and R_y--the smaller these resistance values, the better the channel performs.

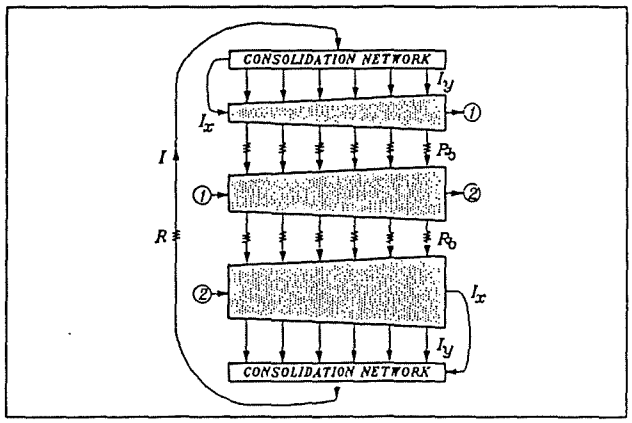

FIGURE 6 — GLOBAL NETWORK (OVERLAP n=6 SHOWN)

OPEN CIRCUIT RELATIONS

When the load current $I = O$ (open circuit), the local solution given by equations (26) through (29) reduces to:

$$E_x = -\frac{(<\beta> + t)<uB>}{G + t^2 + r_b} \tag{62}$$

$$<E_y> = \frac{(t<\beta> + t^2 + r_b)<uB>}{G + t^2 + r_b} \tag{63}$$

$$<J_x> = -\frac{<\sigma> t <uB>}{G + t^2 + r_b} \tag{64}$$

$$J_y = -\frac{<\sigma><uB>}{G + t^2 + r_b} \tag{65}$$

By taking ratios of the various equations above, one gets

$$\frac{E_x}{J_y} = \frac{<\beta> + t}{<\sigma>} \tag{66}$$

$$\frac{<J_x>}{J_y} = t \tag{67}$$

$$-\frac{<E_y>}{E_x} = t + \frac{r_b}{<\beta> + t} = T \tag{68}$$

where t is the tangent of the link overlap angle θ (see Figure 2) and T is the tangent of the equipotential overlap angle Φ given by

$$T = \tan\Phi = \frac{Np}{H} = -\frac{<E_y>}{E_x} \tag{69}$$

where N is the equipotential overlap. All of these equations apply to Faraday generators since $I = O$ automatically holds. In addition, these equations will prove useful later in designing experiments to measure $<\sigma>$ and $<\beta>$.

FARADAY MODE

For Faraday generators, the formulas derived in the previous sections greatly simplify since $n = I = I_x = 0$. When dealing with Faraday generators, it is convenient to introduce standard Faraday notation: $I_f = I_b$, $R_f = R_b$, and $r_f = r_b$. For Faraday operation, the lumped circuit network decouples to an array of Faraday loops. A typical Faraday loop is shown in Figure 7.

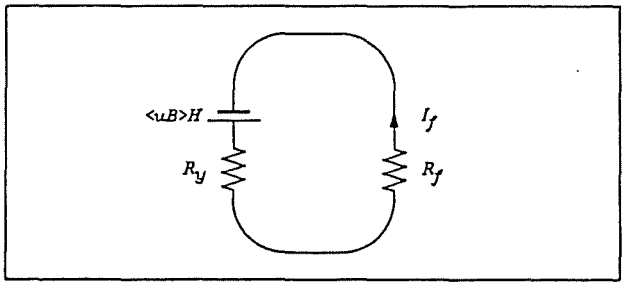

FIGURE 7 — FARADAY LOOP

For Faraday operation, equation (57) reduces to

$$<uB> H = V_f + I_f R_y \tag{70}$$

The open circuit Faraday voltage V_{foc} is obtained by setting $I_f = 0$ in the above equation:

$$V_{foc} = <uB> H \tag{71}$$

Consequently, equation (70) can be rewritten as follows

$$V_f = V_{foc} - I_f R_y \tag{72}$$

The Faraday voltage must also satisfy the relation

$$V_f = -<E_y> H = I_f R_f \tag{73}$$

where R_f is the external Faraday resistance. Thus, equation (70) becomes

$$V_{foc} = <uB> H = I_f (R_f + R_y) \tag{74}$$

A local Faraday load factor k can be defined by

$$k = \frac{V_f}{V_{foc}} = \frac{<E_y>}{<uB>} = \frac{R_f}{R_y + R_f} \tag{75}$$

From the definitions of k, r_f, and R_y it follows that

$$k = \frac{r_f}{G + r_f} \tag{76}$$

$$1 - k = \frac{G}{G + r_f} \tag{77}$$

where in general the nonuniformity factor G depends on generator loading k.

For Faraday generators, the local solution given by equations (26) through (29) reduces to

$$E_x = -\frac{<\beta><uB>}{G + r_f} = -(1-k)\frac{<\beta><uB>}{G} \tag{78}$$

$$<E_y> = \frac{r_f <uB>}{G + r_f} = k <uB> \tag{79}$$

$$<J_x> = 0 \tag{80}$$

$$J_y = -\frac{<\sigma><uB>}{G + r_f} = -(1-k)\frac{<\sigma><uB>}{G} \tag{81}$$

Essentially, parameter k replaces parameter r_f in the Faraday equations.

The power relations given by equations (43) through (46) reduce for Faraday operation to the following relations:

$$\Delta P = I_f V_f = I_f^2 R_f \tag{82}$$

$$\Delta P_M = I_f V_{foc} \tag{83}$$

$$\Delta P_J = I_f (V_{foc} - V_f) \tag{84}$$

The local solution simplifies even further when r_f or equivalently ratio $G/<\sigma>$ does not depend on generator loading. In this case, the short circuit Faraday

current I_{fsc} can be found by setting $V_f = 0$ in equation (72) and using equations (59) and (71) to get:

$$I_{fsc} = \frac{V_{foc}}{R_y} = \frac{\langle\sigma\rangle A_c \langle uB\rangle}{G} \tag{85}$$

From equations (72), (73), (75), (82), and (85), it follows that

$$V_f = kV_{foc} \tag{86}$$

$$I_f = \frac{V_{foc} - V_f}{R_y} = \frac{V_{foc} - kV_{foc}}{R_y} = (1-k)I_{fsc} \tag{87}$$

$$R_f = \frac{V_f}{I_f} = \frac{kV_{foc}}{(1-k)I_{fsc}} = \frac{k}{1-k}R_y \tag{88}$$

$$\Delta P = V_f I_f = k(1-k)V_{foc}I_{fsc} \tag{89}$$

Clearly, Faraday power is maximal when $k = 1/2$ or, equivalently, $R_f = R_y$ or $r_f = G$. The condition that R_y be independent of generator loading is equivalent to the local Faraday load line being linear, as shown in Figure 8.

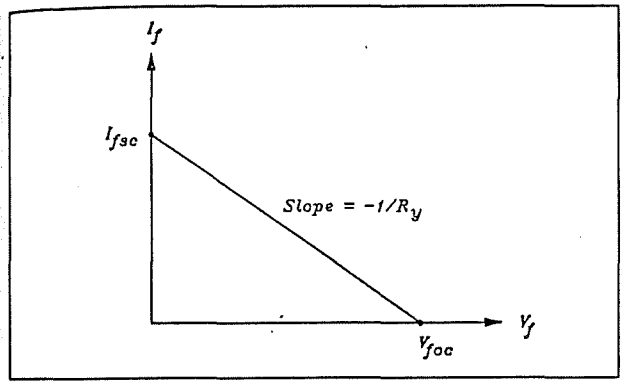

FIGURE 8 — LOCAL FARADAY LOAD LINE

DIAGONAL MODE

The local Hall solution can be obtained from the local solution by integrating equation (26) over one pitch:

$$V_h = -\int_p E_x dx = -pE_x$$

$$= -\left[\frac{p(\langle\beta\rangle + t)\langle uB\rangle}{G + t^2 + r_b}\right] - \left[\frac{G + \langle\beta\rangle^2 + r_b}{G + t^2 + r_b}\frac{p}{\langle\sigma\rangle A}\right] I \tag{90}$$

If the above bracketed expressions can be regarded as reasonably constant over a load sweep, then equation (90) can be rewritten as

$$V_h = V_{hoc} - IR_g \tag{91}$$

Where V_{hoc} is the open circuit Hall voltage per pitch given by

$$V_{hoc} = \frac{p(\langle\beta\rangle + t)\langle uB\rangle}{G + t^2 + r_b} \tag{92}$$

and R_g is the generator internal resistance per pitch given by

$$R_g = \frac{G + \langle\beta\rangle^2 + r_b}{G + t^2 + r_b}\frac{p}{\langle\sigma\rangle A} \tag{93}$$

The local short circuit current I_{lsc} is obtained by setting $V_h = 0$ in equation (91):

$$I_{lsc} = \frac{V_{hoc}}{R_g} = \frac{\langle\sigma\rangle A(\langle\beta\rangle + t)\langle uB\rangle}{G + \langle\beta\rangle^2 + r_b} \tag{94}$$

Using the above relation, equation (91) can be rewritten in the following alternate form

$$V_h = I_{lsc}R_g - IR_g = (I_{lsc} - I)R_g \tag{95}$$

In practice, V_{hoc} and I_{lsc} are obtained from load line extrapolations as shown in Figure 9 and R_g is obtained from equation (94) or directly from the slope of the experimental load line.

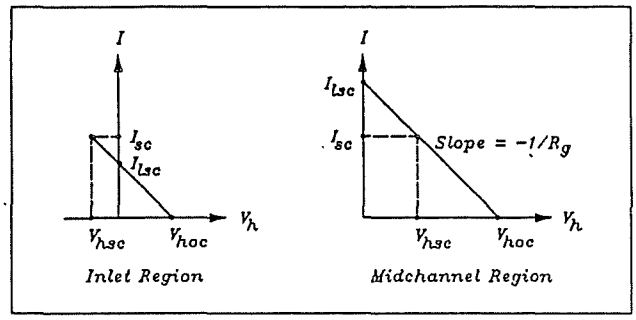

FIGURE 9 — LOCAL HALL LOAD LINES

The short circuit Hall voltage for one pitch, denoted by V_{hsc}, can be found from equation (95) by setting $I = I_{sc}$:

$$V_{hsc} = (I_{lsc} - I_{sc})R_g \tag{96}$$

Clearly V_{hsc} can become negative at any location where the global short circuit current I_{sc} exceeds the local short circuit current I_{lsc}. This is exactly the situation that occurs at the channel inlet where both $\langle\beta\rangle$ and B are relatively small, and hence so is I_{lsc}. Consequently, it follows from equation (95) that V_h can become negative (Hall field reversal) in the inlet region at large load currents I. Furthermore, the Hall field reversal is usually accompanied by a Faraday field reversal due to excessive downstream axial currents I_x (see equations (57) and (58)). From equation (94), it appears that the only practical remedy is to increase the link overlap and decrease the link resistance in the inlet region.

For diagonal connections, the Hall load resistance R can be thought of as being distributed over the entire channel length as follows:

$$R = \frac{V}{I} = \frac{\Sigma V_h}{I} = \Sigma\frac{V_h}{I} = \Sigma R_h \tag{97}$$

where $R_h = \Delta R$ is the load resistance per pitch defined by

$$R_h = \frac{V_h}{I} \tag{98}$$

Consequently, it follows from equations (91) and (98) that the open circuit Hall voltage per pitch is given by

$$V_{hoc} = V_h + IR_b = IR_h + IR_g = I(R_h + R_g) \tag{99}$$

A local Hall load factor k can be defined by

$$k = \frac{V_h}{V_{hoc}} = \frac{R_h}{R_h + R_g} \tag{100}$$

Although the same symbol k is used to represent the (local) Hall and Faraday load factors, there should be little confusion since it will usually be clear from the context whether the generator is of the diagonal type or Faraday type.

From equations (91), (94), (98), and (100), it follows that

$$V_h = kV_{hoc} \tag{101}$$

$$I = \frac{V_{hoc} - V_h}{R_g} = \frac{V_{hoc} - kV_{hoc}}{R_g} = (1-k)I_{isc} \tag{102}$$

$$R_h = \frac{V_h}{I} = \frac{kV_{hoc}}{(1-k)I_{isc}} = \frac{k}{1-k}R_g \tag{103}$$

$$\Delta P_h = V_h I = k(1-k)V_{hoc}I_{isc} \tag{104}$$

Clearly, the Hall power ΔP_h extracted per pitch is maximal when $k = 1/2$ or, equivalently, $V_h = (1/2)V_{hoc}$, $I = (1/2)I_{isc}$, or $R_h = R_g$. However, the net power $\Delta P = \Delta P_h + \Delta P_b$ is not necessarily maximal at this condition. A major problem with diagonal operation is that it is virtually impossible to maintain the optimum (local) load factor at all locations since I_{isc} varies considerably along the channel. However, by varying the link overlap and link resistance properly along the channel, the variation in I_{isc} can be reduced substantially, and the channel can be operated with local load factors near optimum ($k = 1/2$).

FARADAY OPTIMIZATION

For Faraday generators, it follows from equations (71), (85), and (89) that the electrical power extracted per pitch is given by

$$\Delta P = k(1-k)\frac{p\langle\sigma\rangle A\langle uB\rangle^2}{G} \tag{105}$$

Although ΔP always maximizes at $k = 1/2$ when the other quantities on the right-hand side of equation (105) are fixed, ΔP also depends strongly on $\langle uB\rangle$ and ratio $G/\langle\sigma\rangle$. Thus, $\langle uB\rangle$ and ratio $G/\langle\sigma\rangle$ are two good measures of combustor performance since Faraday power varies directly with the square of $\langle uB\rangle$ and inversely with the ratio $G/\langle\sigma\rangle$.

It follows immediately from equation (47) that the Faraday connection ($t = 0$) produces maximum power among all diagonal connections at open circuit conditions ($I = 0$). A related question is whether tapping the Hall field via an external load would result in more power produced by a Faraday generator. Since equations (47) through (52) apply to this situation (with $t = 0$), after simplifying one gets:

$$\Delta P = \frac{p}{\langle\sigma\rangle A}\frac{r_l\langle\sigma\rangle^2 A^2\langle uB\rangle^2 + (G - r_l)\langle\beta\rangle\langle\sigma\rangle A\langle uB\rangle I - [(G + r_l)^2 + G\langle\beta\rangle^2]I^2}{(G + r_l)^2} \tag{106}$$

Upon differentiating the above relation with respect to I (assuming the other terms on the right-hand side do not depend on I) and setting the result equal to zero, one obtains the optimum Hall load current I:

$$I = \frac{(G - r_l)\langle\beta\rangle\langle\sigma\rangle A\langle uB\rangle}{2[(G + r_l)^2 + G\langle\beta\rangle^2]} \tag{107}$$

However, it has already been shown that an optimally loaded Faraday generator operates at load factor $k = 1/2$ or, equivalently, $r_l = G$. In this case, it follows from equation (107) that the optimal Hall load current $I = 0$ and no additional power can be realized by tapping the Hall field.

For later reference, it is noted that the optimally loaded Faraday generator (at $k = 1/2$) has average electric field components given by

$$E_x = -\frac{\langle\beta\rangle\langle uB\rangle}{2G} \tag{108}$$

$$\langle E_y\rangle = -\frac{\langle uB\rangle}{2} \tag{109}$$

$$\langle J_x\rangle = 0 \tag{110}$$

$$J_y = -\frac{\langle\sigma\rangle\langle uB\rangle}{2G} \tag{111}$$

$$\Delta P = \frac{p\langle\sigma\rangle A\langle uB\rangle^2}{4G} = \frac{[\langle uB\rangle H]^2}{4R_y} \tag{112}$$

DIAGONAL OPTIMIZATION

For diagonal generators, it follows from equations (92), (94), and (104) that the Hall load power extracted per pitch is given by

$$\Delta P_h = k(1-k)\frac{p\langle\sigma\rangle A(\langle\beta\rangle + t)^2\langle uB\rangle^2}{(G + t^2 + r_b)(G + \langle\beta\rangle^2 + r_b)} \tag{113}$$

Clearly, ΔP_h maximizes at $k = 1/2$ when the other terms on the right-hand side of equation (113) are fixed. However, ΔP_h also depends strongly on $\langle uB\rangle$, ratio $G/\langle\sigma\rangle$, and parameter t.

The value of parameter t that maximizes ΔP_h can be found by differentiating equation (113) with respect to t (assuming the other terms on the right-hand side do not depend on t). Setting this derivative equal to zero, one obtains the optimal t:

$$t = \frac{G + r_b}{\langle\beta\rangle} \tag{114}$$

In reality, the degree of polarization depends on t and hence so do G and r_b. Thus, an iterative procedure is required, where the optimal t given by equation (114) must be successively updated as G and r_b vary in response to changes in t until equilibrium is established and equation (114) is satisfied on a steady-state basis. Then and only then is the optimal

t that maximizes Hall power determined.[2] The optimal (diagonal) link parameter t will be denoted by t^* in the remainder of this paper.

From equation (94) and (114), it follows that the local short circuit current at the optimal link overlap is given by

$$I_{sc} = \frac{\langle\sigma\rangle A \langle uB\rangle}{\langle\beta\rangle} \tag{115}$$

Although the local short circuit current given by equation (115) would likely be moderately uniform along the channel, the optimal t given by equation (114) is unrealistically large at the channel entrance due to excessively small Hall parameters occurring there. Nevertheless, the channel needs to be reconfigured at the inlet to increase power production there. This could be accomplished by increasing the link overlap and reducing the ballast resistance as much as possible.

At the optimal link overlap, it follows from equations (102) and (115) that the load current I is given by

$$I = (1-k)\frac{\langle\sigma\rangle A \langle uB\rangle}{\langle\beta\rangle} \tag{116}$$

where k is the local Hall load factor. Plugging the above expression for I into equations (26) through (29) and using relation (114), one obtains the local solution at the optimal link overlap:

$$E_x = -k\frac{\langle\beta\rangle\langle uB\rangle}{G+r_b} \tag{117}$$

$$\langle E_y\rangle = \left[r_b + k\left(G+\langle\beta\rangle^2 + \frac{\langle\beta\rangle^2 r_b}{G+r_b}\right)\right]\frac{\langle uB\rangle}{G+\langle\beta\rangle^2+r_b} \tag{118}$$

$$\langle J_x\rangle = (1-2k)\frac{\langle\sigma\rangle\langle\beta\rangle\langle uB\rangle}{G+\langle\beta\rangle^2+r_b} \tag{119}$$

$$J_y = -\left(1-k\frac{G-\langle\beta\rangle^2+r_b}{G+r_b}\right)\frac{\langle\sigma\rangle\langle uB\rangle}{G+\langle\beta\rangle^2+r_b} \tag{120}$$

Although these formulas are somewhat complicated, they greatly simplify when $k = 1/2$ or $r_b = 0$. Maximum Hall power is extracted when both $k = 1/2$ and $r_b = 0$. Thus, it follows from equations (117) through (120) that a diagonal generator optimally configured for maximum Hall power production has average electric field components given by

$$E_x = -\frac{\langle\beta\rangle\langle uB\rangle}{2G} \tag{121}$$

$$\langle E_y\rangle = \frac{\langle uB\rangle}{2} \tag{122}$$

$$\langle J_x\rangle = 0 \tag{123}$$

$$J_y = -\frac{\langle\sigma\rangle\langle uB\rangle}{2G} \tag{124}$$

$$\Delta P = \frac{P\langle\sigma\rangle A\langle uB\rangle^2}{4G} = \frac{[\langle uB\rangle H]^2}{4R_y} \tag{125}$$

At this optimal condition, the electrical power extracted per pitch depends only on $\langle uB\rangle$ and ratio $G/\langle\sigma\rangle$, as was the case for Faraday generators (see equation (105)).

Interestingly, electric field equations (121) through (125) for the optimally configured and loaded diagonal generator have the same form as the corresponding field equations (108) through (112) for the optimally loaded Faraday generator. The only reasonable conclusion possible is that the equilibrium values for the plasma/slag properties will be essentially the same in both cases and the electric fields produced by each type of generator will be identical for all practical purposes. In particular, the power extracted per pitch for each locally optimized connection, whether it be Faraday or diagonal, will be essentially the same. Thus, on a local basis, there is no inherent advantage of Faraday over diagonal or vice versa. On a global basis, however, there may be advantages of one type of connection over the other due to difficulties in simultaneously optimizing the generator at all locations. This problem is particularly apparent for diagonal connections where the local short circuit current I_{sc} usually varies along the channel, and consequently, it becomes impossible to operate the generator at a local load factor $k = 1/2$ at all locations (see equation (102)).

RECOMMENDED EXPERIMENTS

The following experiments are needed to estimate a few key channel parameters not currently being measured. Once these key parameters are known, many other channel parameters of interest can easily be calculated. For best results, the combustor should be operated at nominal baseline conditions during these experiments.

Measuring $\langle u\rangle$

The average plasma velocity $\langle u\rangle$ under no load can be determined from an open circuit Faraday test (no external links). Since unacceptably large Faraday voltages may occur at full magnetic field strength, this test should be run at low B fields. Assuming the B field is constant on any cross section, one obtains from equation (71) the following relation:

$$V_{foc} = \langle uB\rangle H = \langle u\rangle BH \tag{126}$$

Using this relation, $\langle u\rangle$ can be easily calculated from measurements of V_{foc} and B. Once $\langle u\rangle$ is known, V_{foc} at full magnetic field strength can be readily calculated from equation (126).

Measuring $\langle\mu\rangle$

The average electron mobility $\langle\mu\rangle$ can be determined from an open circuit diagonal test (no external load). Since unacceptably large Hall voltages may occur at full magnetic field strength, this test should be run at low B fields. Assuming the B field is constant on any cross section, one gets

$$\langle\beta\rangle = \langle\mu B\rangle = \langle\mu\rangle B \tag{127}$$

From equations (66) and (127), it follows that

$$\frac{E_x}{J_y} = \frac{\langle\beta\rangle}{\langle\sigma\rangle} + \frac{t}{\langle\sigma\rangle} = \frac{\langle\mu\rangle}{\langle\sigma\rangle}B + \frac{t}{\langle\sigma\rangle} \tag{128}$$

A magnetic field sweep at low B values is needed to determine the slope and intercept of the above line. This test should be performed early in the test

sequence while the channel is in a relatively unpolarized state. The prepower $\langle\sigma\rangle$ is determined from the intercept, and using this value, the prepower $\langle\mu\rangle$ is determined from the slope. The electron mobility is not expected to change much under power generation conditions. As a bonus, this test establishes the prepower $\langle\sigma\rangle$ for diagonal generators without the need for a separate prepower conductivity test (in effect, the generator becomes its own power supply). This test can also be run for Faraday generators, but a separate conductivity test is needed to determine the prepower $\langle\sigma\rangle$ since the intercept in equation (128) is always zero ($i=0$) for Faraday connections. Once $\langle\mu\rangle$ is known, $\langle\beta\rangle$ at full magnetic field strength can be readily calculated from equation (127).

Measuring R_y

The (per pitch) transverse resistance R_y under power can be determined from a Faraday load sweep. This test is needed to determine how sensitive R_y or equivalently ratio $G/\langle\sigma\rangle$ is to generator loading. If R_y does not depend on generator loading, then the Faraday load lines are linear, as shown in Figure 8, and the analysis of Faraday generators becomes considerably easier. The resistance R_y is determined from the slope of the load line, and V_{foc} and I_{fsc} are determined from the intercepts (see Figure 8). The entire Faraday generator should be loaded at approximately the same local load factor k to avoid rapid axial changes that may invalidate the simplifying assumptions stated at the beginning of this paper. As a bonus, this test also determines V_{foc}, I_{fsc}, and $\langle u\rangle$ (see equation (126)). Resistance R_y also can be estimated by the methods described in the next section.

PARAMETER ESTIMATION

Once $\langle u\rangle$ and $\langle\mu\rangle$ have been experimentally determined, many other important channel properties can be estimated from them using routine experimental data. For example, it has already been mentioned that the average Hall parameter $\langle\beta\rangle$ can be calculated from equation (127) once $\langle\mu\rangle$ is known. Methods for estimating other important parameters are given below.

Estimating $\langle\sigma\rangle$

The average conductivity $\langle\sigma\rangle$ under power can be easily computed at any axial location once $\langle\beta\rangle$ is known. It follows from equation (22) that

$$\langle\sigma\rangle = \frac{\langle J_x\rangle + \langle\beta\rangle J_y}{E_x} \tag{129}$$

For best results, local average values (over several electrodes) should be used for E_x, $\langle J_x\rangle$, and J_y in the above formula.

Estimating I_s

The (average) slag axial leakage current I_s under power can be computed at any axial location once $\langle\sigma\rangle$ and $\langle\sigma_p\rangle$ are known. The average plasma conductivity $\langle\sigma_p\rangle$ can be estimated from prepower conductivity or electron mobility tests. It is convenient to split the conductivity into two parts:

$$\sigma = \sigma_p + \sigma_s \tag{130}$$

where σ_p is the plasma contribution ($\sigma_p=0$ in the slag layers) and σ_s is the slag contribution ($\sigma_s=0$ in the plasma). Thus

$$\langle\sigma_s\rangle = \langle\sigma\rangle - \langle\sigma_p\rangle \tag{131}$$

The average slag resistance per pitch is given by

$$R_s = \frac{p}{\langle\sigma_s\rangle A} \tag{132}$$

and the (local average) slag leakage current is given by

$$I_s = -\frac{V_h}{R_s} = \langle\sigma_s\rangle A E_x \tag{133}$$

where a negative value indicates an upstream leakage current. For best results, local average values (over several electrodes) should be used for E_x in the above formula.

Estimating I_p

The average plasma current I_p under power is easily computed at any axial location once I_s is known. It is convenient to split the net axial current into two parts:

$$I_x = I_p + I_s \tag{134}$$

where I_p is the plasma contribution and I_s is the slag contribution (recall that I_x can be computed easily using equation (21)). It follows immediately from equation (134) that

$$I_p = I_x - I_s \tag{135}$$

Since I_s is normally negative in the adopted coordinate system (indicating an upstream leakage current), it is seen that the I_s term usually acts to increase the estimated value of I_p in the above formula. While it is true that large upstream leakage currents tend to be associated with large downstream plasma currents, the real cause for both effects is the large transverse nonuniformities that exist in coal-fired MHD channels. These nonuniformities can be measured via the net nonuniformity factor G.

Estimating G

The net nonuniformity factor G under power is easily computed at any axial location once $\langle u\rangle$, $\langle\beta\rangle$, and $\langle\sigma\rangle$ are known. It follows from equation (12) that

$$G = \frac{\langle\beta\rangle\langle J_x\rangle - \langle\sigma\rangle(\langle uB\rangle - \langle E_y\rangle)}{J_y} \tag{136}$$

For best results, local average values (over several electrodes) should be used for $\langle E_y\rangle$, $\langle J_x\rangle$, and J_y in the above formula.

Estimating $G/\langle\sigma\rangle$

Ratio $G/\langle\sigma\rangle$ is a crucial indicator of generator performance and obviously can be computed once G and $\langle\sigma\rangle$ are known. The formulas previously given for estimating G and $\langle\sigma\rangle$ depend on knowing $\langle u\rangle$ and $\langle\beta\rangle$. However, when $\langle J_x\rangle$ is small in comparison to J_y, ratio $G/\langle\sigma\rangle$ can be accurately estimated without knowing $\langle\beta\rangle$. This can be seen by solving equation (11) for $\langle\beta\rangle$, substituting this result into equation (136), and then solving for ratio $G/\langle\sigma\rangle$ as follows:

$$\frac{G}{\langle\sigma\rangle} = \frac{E_x\langle J_x\rangle}{J_y^2} - \frac{\langle uB\rangle - \langle E_y\rangle}{J_y} - \frac{\langle J_x\rangle^2}{\langle\sigma\rangle J_y^2} \qquad (137)$$

The only quantity on the right-hand side of equation (137) that depends on knowing $\langle\beta\rangle$ for its estimation is $\langle\sigma\rangle$. However, if $\langle J_x\rangle$ is small in comparison to J_y, then the last term in equation (137) is negligible; hence, the ratio $G/\langle\sigma\rangle$ can be accurately estimated from the first two terms. In this case, only $\langle u\rangle$ and routine experimental data are needed to estimate ratio $G/\langle\sigma\rangle$. It should be noted that $\langle J_x\rangle$ is usually small in comparison to J_y for diagonal generators operating near their peak power condition and, of course, for all Faraday generators where $\langle J_x\rangle = 0$. Once ratio $G/\langle\sigma\rangle$ is known, the internal resistance R_y can be easily estimated via equation (59).

Estimating t^*

The estimate for the optimal link parameter t^* for diagonal connections given by equation (114) requires knowing $\langle\beta\rangle$. In many important applications, however, this dependence on $\langle\beta\rangle$ is fairly weak. This can be seen by rewriting equation (114) using equation (129) as follows:

$$t^* = \frac{G + r_b\langle\sigma\rangle}{\langle\sigma\rangle}\frac{\langle\sigma\rangle}{\langle\beta\rangle} = \left[\frac{G}{\langle\sigma\rangle} + \frac{A_s R_b}{H}\right]\left[\frac{\langle J_x\rangle}{\langle\beta\rangle} + J_y\right]E_x^{-1} \qquad (138)$$

The first bracketed expression can be estimated accurately without knowing $\langle\beta\rangle$ when $\langle J_x\rangle \ll J_y$. The same is true for the second bracketed expression when $\langle J_x\rangle/\langle\beta\rangle \ll J_y$. When both of these conditions occur, as is typical at peak power diagonal operation or any Faraday operation, t^* can be accurately estimated by either equation (114) or equation (138) without knowing $\langle\beta\rangle$. It should be noted that the optimal t for diagonal connections can be estimated from Faraday test data provided the appropriate diagonal ballast resistance is used in equations (114) and (138).

COMPUTATIONAL RESULTS

The formulas developed in the previous sections will now be applied to recent CDIF experimental data. CDIF tests 89-DIAG-11, 89-DIAG-12, and 88-FARA-1 were selected for analysis since each test generated at least 2 hours of data with peak powers over 1.6 MW, and each test included a prepower conductivity test.

Table 1 lists the nominal plasma properties and channel dimensions assumed for these tests at six selected axial locations (electrodes 40, 80, 120, 160, 200, and 240). The average axial velocities in Table 1 are representative of those determined from link current cross-correlations[8] and from 3-D model calculations[9] for the CDIF channel. The average Hall parameters were taken from reference 9. Standard MKS units are assumed throughout this paper.

Table 1 -- Assumed plasma properties and channel dimensions.

NUM	p	W	H	B	$\langle\beta\rangle$	$\langle u\rangle$
40	.01524	.1158	.2414	2.38	.88	1385
80	.01524	.1425	.2517	2.91	1.23	1420
120	.01524	.1692	.2621	2.90	1.44	1420
160	.01524	.1959	.2724	2.84	1.67	1405
200	.01524	.2226	.2827	2.72	1.82	1390
240	.01524	.2493	.2930	2.32	1.62	1370

Tables 2 through 6 summarize the measured inputs and computed outputs for each selected test condition. In the end regions (electrodes 40 and 240), the calculated data is somewhat erratic and unreliable since the simplifying assumptions on which the models depend tend to fail there. In extreme cases, this results in calculated values that are physically impossible, such as a nonuniformity factor less than one. In such cases, each obviously erroneous value is replaced by an "*" in the tables. Even if an "*" does not appear in a given table, the entries in the end regions are suspect, especially at low Hall voltage conditions (primarily in Table 2). The notation used in the tables is the same as that used in the text, except that n^* is introduced to denote the optimal link overlap. The optimal link overlap n^* is computed from the optimal link parameter t^* via equations (18) and (114). The first column in each table is the electrode number.

For test 89-DIAG-11, three test conditions--representing a load sweep--were selected for analysis. The relevant data for this load sweep appears in Tables 2 through 4. The local Hall load factor k clearly increases at each location as the global loading increases. Furthermore, at each load condition, the axial profile for the local load factor assumes approximately a parabolic shape with the maximum load factor occurring in the midchannel region and the minimum load factor occurring in the end regions. This characteristic profile is essentially due to the use of a constant link overlap and a constant link resistance in a channel with axially varying magnetic fields and plasma/slag properties. From Tables 2 through 4, it is evident that the slag leakage current I_s increases in magnitude with increasing Hall voltage, while the opposite trend holds for the plasma current I_p. Both currents are large at the peak power condition (Table 3) due to the large transverse nonuniformities occurring in the channel (caused in part by cathode wall polarization). The severity of these transverse nonuniformities at any axial location is measured by the net nonuniformity factor G. However, the estimates for G and $\langle\sigma\rangle$ appearing in the tables are somewhat erratic and unreliable in the end regions. Ratio $G/\langle\sigma\rangle$ appears to be more stable over a load sweep than either G or $\langle\sigma\rangle$. Consequently, the transverse resistance R_y at any axial location appears to be relatively insensitive to generator loading. Furthermore, R_y appears to be relatively constant along the entire length of the

Table 2 -- Measured electrical inputs and computed outputs for test 89-DIAG-11, condition 12 (iron test). Global electrical parameters were 1722 V, 350 A, and 0.93 MWe.

NUM	R_b	$\langle\sigma_p\rangle$	E_x	$\langle E_y\rangle$	J_y	I_x	I_p	I_s	G	$\langle\sigma\rangle$	$\frac{\sigma}{\langle\sigma\rangle}$	R_x	R_y	k	n^*
40	6	8.5	70	280	-9000	175	238	-63	*	*	0.36	*	49.4	0.12	*
80	6	6.0	-520	780	-7900	161	237	-75	3.6	10.0	0.35	0.042	41.1	0.30	55
120	6	4.7	-700	800	-6400	168	263	-94	3.2	7.7	0.41	0.044	41.5	0.33	43
160	6	4.1	-880	875	-5200	179	271	-92	2.5	6.1	0.42	0.047	38.4	0.32	32
200	6	3.5	-795	700	-4000	201	283	-82	2.5	5.1	0.49	0.047	40.7	0.28	29
240	6	3.4	-480	500	-2900	229	224	5	1.3	3.3	0.39	0.064	29.9	0.13	18

Table 3 -- Measured electrical inputs and computed outputs for test 89-DIAG-11, condition 10 (iron test). Global electrical parameters were 4908 V, 208 A, and 1.47 MWe.

NUM	R_b	$\langle\sigma_p\rangle$	E_x	$\langle E_y\rangle$	J_y	I_x	I_p	I_s	G	$\langle\sigma\rangle$	$\frac{\sigma}{\langle\sigma\rangle}$	R_x	R_y	k	n^*
40	6	8.5	-595	740	-9100	31	82	-51	3.1	11.6	0.27	0.047	37.1	0.47	66
80	6	6.0	-1280	1330	-8600	3	104	-101	2.7	8.2	0.32	0.052	37.6	0.58	41
120	6	4.7	-1560	1400	-7300	1	141	-140	2.5	6.7	0.37	0.051	37.8	0.60	35
160	6	4.1	-1795	1500	-6500	-5	187	-192	2.4	6.1	0.39	0.047	35.3	0.62	30
200	6	3.5	-1680	1340	-5500	3	260	-257	2.6	5.9	0.44	0.041	36.8	0.63	31
240	6	3.4	-1180	1035	-4100	37	192	-156	2.5	5.2	0.48	0.040	37.4	0.55	35

Table 4 -- Measured electrical inputs and computed outputs for test 89-DIAG-11, condition 11 (iron test). Global electrical parameters were 7527 V, 79 A, and 1.15 MWe.

NUM	R_b	$\langle\sigma_p\rangle$	E_x	$\langle E_y\rangle$	J_y	I_x	I_p	I_s	G	$\langle\sigma\rangle$	$\frac{\sigma}{\langle\sigma\rangle}$	R_x	R_y	k	n^*
40	6	8.5	-1195	1190	-8500	-86	-75	-11	2.5	8.8	0.28	0.062	38.8	0.78	52
80	6	6.0	-2000	1830	-8700	-129	-47	-82	2.4	7.1	0.34	0.059	38.9	0.82	37
120	6	4.7	-2230	1845	-7800	-142	33	-176	2.5	6.5	0.38	0.053	38.9	0.85	34
160	6	4.1	-2430	1970	-7500	-167	137	-304	2.4	6.4	0.38	0.044	34.5	0.86	31
200	6	3.5	-2285	1830	-6600	-167	253	-420	2.6	6.4	0.41	0.038	34.1	0.86	32
240	6	3.4	-1715	1440	-5200	-138	189	-328	2.6	6.0	0.43	0.035	33.3	0.84	36

Table 5 -- Measured electrical inputs and computed outputs for test 89-DIAG-12, condition 5 (iron test). Global electrical parameters were 4979 V, 239 A, and 1.89 MWe.

NUM	R_b	$\langle\sigma_p\rangle$	E_x	$\langle E_y\rangle$	J_y	I_x	I_p	I_s	G	$\langle\sigma\rangle$	$\frac{\sigma}{\langle\sigma\rangle}$	R_x	R_y	k	n^*
40	6	9.3	-700	1035	-11000	25	89	-63	2.5	12.5	0.20	0.044	27.3	0.48	55
80	6	6.8	-1500	1600	-10700	-17	106	-123	2.2	9.1	0.24	0.047	28.1	0.60	36
120	6	5.4	-1685	1600	-9200	-22	184	-206	2.3	8.2	0.28	0.042	28.8	0.63	33
160	6	4.4	-1615	1485	-7700	-14	307	-321	2.7	8.1	0.33	0.035	30.3	0.64	35
200	6	3.9	-1500	1315	-6700	-11	399	-410	3.1	8.2	0.37	0.029	31.1	0.66	37
240	6	3.7	-1060	1035	-5000	30	305	-275	3.0	7.3	0.41	0.029	31.6	0.59	42

Table 6 -- Measured electrical inputs and computed outputs for test 88-FARA-1, condition 5 (noniron test). Global electrical parameters were 4308 V and 1.60 MWe.

NUM	R_f	$\langle\sigma_p\rangle$	E_x	$\langle E_y\rangle$	J_y	I_x	I_p	I_s	G	$\langle\sigma\rangle$	$\frac{\sigma}{\langle\sigma\rangle}$	R_x	R_y	k	n^*
40	24.0	6.0	-770	1320	-7400	0	53	-53	2.3	8.5	0.27	0.064	36.5	0.40	47
80	27.5	5.4	-1030	1785	-7500	0	131	-131	2.8	9.0	0.31	0.047	36.3	0.43	44
120	30.3	4.9	-1145	1840	-6100	0	141	-141	2.9	7.7	0.37	0.045	38.0	0.45	40
160	32.9	4.6	-1445	1860	-5100	0	100	-100	2.5	5.9	0.42	0.048	38.1	0.47	30
200	36.0	4.3	-1420	1840	-4500	0	131	-131	2.5	5.8	0.43	0.042	35.9	0.49	30
240	40.0	4.0	-930	1440	-2900	0	71	-71	3.0	5.1	0.6	0.041	46.2	0.45	41

channel. Finally, the estimated value for the optimal link overlap n^* at any axial location appears to be relatively insensitive to generator loading, except in the end regions where all estimates are somewhat unreliable.

For test 89-DIAG-12, only the peak power condition was selected for analysis. Table 5 lists the relevant data for this test condition. Ratios $G/\langle\sigma\rangle$ and resistances R_y for this test appear to be significantly smaller than those in the previous test, possibly accounting for the increased power observed for this test over the previous test. Interestingly, the plasma and slag leakage currents also appear larger than those for the corresponding condition in the previous test (Table 3). However, the estimates for currents I_p and I_s are not as reliable as those for the ratio $G/\langle\sigma\rangle$ and resistance R_y since the former depend on knowing both $\langle\beta\rangle$ and $\langle\sigma_p\rangle$ while the latter depend on knowing only $\langle u\rangle$ (and routine CDIF data). The estimated values for the optimal link overlaps n^* are similar to those computed from the previous test.

For test 88-FARA-1 (the most recent Faraday test with prepower conductivity measurements at the time of this paper), the peak power condition was selected for analysis. Table 6 lists the relevant data for this test condition. The parameter estimates appear to be similar to those computed for test 89-DIAG-11 except that the slag leakage currents are somewhat smaller in the rear half of the channel for the Faraday test. There appears to be a good impedance match between the external resistance R_f and the internal resistance R_y for this test, with local load factors k near optimum. The optimal link overlaps n^* for diagonal connections indicated by this Faraday test are similar to those calculated from the three diagonal tests.

The estimated values for the axial currents I_s and I_p given in the tables appear to be excessively large in the rear half of the channel, especially at the higher Hall voltage conditions. These estimates depend strongly on knowing the average plasma conductivity $\langle\sigma_p\rangle$, which in this paper was assumed to be the same as the average prepower conductivity. However, this assumption may not be a good one at the higher Hall voltage conditions since the MHD interaction (the mechanical power extracted) increases as the Hall voltage increases.

CONCLUSIONS

From a casual inspection of Tables 2 through 5, it is clear that the link overlap $n = 11$ used in the diagonal tests is far from optimal for the CDIF generator. From the tables, it appears that the optimal link overlap is approximately 30 at midchannel and increases to 40 or more in the end regions. Even the Faraday test data when properly interpreted confirms this conclusion (see Table 6). If the link overlaps were increased to their optimal values, the global load line for diagonal operation would shift to a higher short circuit current I_{sc}^* and a lower open circuit voltage V_{oc}^* as shown in Figure 10. This change should reduce axial stresses somewhat in the channel but may increase transverse stresses by a comparable amount. However, substantially more power is lost through axial slag leakage than through transverse slag leakage, so the recommended change to larger link overlaps should reduce slag power losses overall and increase the net power extracted from the channel.

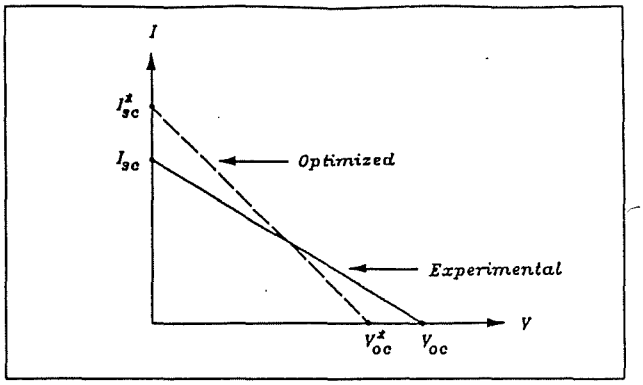

FIGURE 10 — OPTIMIZED GLOBAL HALL LOAD LINE

A key aspect to optimizing diagonal channel performance is matching reasonably well the local short circuit currents I_{lsc} along the entire channel length. It is clear from the experimental data that this match was not achieved for the diagonal tests analyzed in this paper since there were Hall field reversals in the inlet region at low Hall voltages. It is the large mismatch in local short circuit currents that causes the Hall field reversals as indicated in Figure 9. A properly optimized diagonal channel should generate local short circuit currents that are nearly the same everywhere and, thus, approximately equal to the global short circuit current I_{sc}^* as indicated in Figure 11. An exact match in local short circuit currents along the channel is not required--only a reasonable match is needed so the diagonal generator can operate with local Hall load factors k in the range of 0.45 to 0.55 at nearly all locations. For load factors in this range, there is little degradation in power extracted from the optimal load factor $k = 0.5$ (less than 1 percent degradation). Furthermore, operating the generator with local load factors in this range permits the entire generator to function near optimal at the same external load--a critical consideration for diagonal operation.

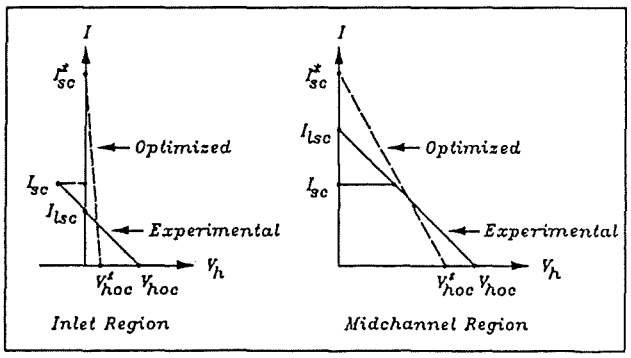

FIGURE 11 — OPTIMIZED LOCAL HALL LOAD LINES

Basically, the presence of coal slag has forced the CDIF generator to operate off-design. If there were no slag layers and no ballast resistors (none would be needed in the absence of coal-induced polarization), the net nonuniformity factor G would be considerably smaller and so would the optimal link parameter t^* given by equation (114). For example, if G and $\langle\beta\rangle$ were approximately 1.25 and 1.47, respectively, at midchannel, then n^* would be approximately 15 at midchannel--in agreement with the way the channel was

originally designed. However, an all peg sidewall design would be needed to implement link overlaps n' as varied as those shown in Tables 2 through 6. When applying equation (114) to obtain the optimal link overlap, one should always bear in mind that an iterative procedure is really required since changing the generator connections will likely change the plasma/slag properties somewhat. The first attempt at generator optimization will probably need additional fine tuning.

For Faraday connections, the end regions also pose special problems but for different reasons. Here, the main problem is obtaining the proper impedance match between the Faraday load R_f and the effective internal resistance R_y'. Up to this point, transverse leakage effects have been ignored. In the end regions, however, the combustor and diffuser provide highly conductive paths for substantial leakage currents between each anode-cathode pair. If this leakage current has effective resistance R_t per pitch, then the effective internal resistance R_y' per pitch is given by

$$R_y' = \frac{R_y R_t}{R_y + R_t} \tag{139}$$

Clearly, R_y' is the equivalent resistance for R_y and R_t connected in parallel. In the midchannel region, R_t is relatively large and probably can be ignored. In this case, R_y' is approximately equal to R_y and matching R_f to R_y is a good strategy. In the end regions, however, R_t is relatively small and cannot be ignored. In this case, one must match R_f to R_y', which is considerably smaller than R_y, to obtain the maximum power transfer to the external load. As the ends of the channel are approached, both R_t and R_y' can become quite small. For this reason, Faraday load profiles must taper to nearly zero at the channel ends. A remedy for this situation is to segment those portions of the combustor and diffuser adjacent to the channel ends. In this way, the effective transverse leakage at the channel ends can be reduced considerably and the effective transverse resistance R_y' increased to the point that significantly greater amounts of power can be extracted in the end regions. A properly segmented combustor and diffuser should increase power extraction in the end regions for a diagonal generator as well, since any reduction in transverse shorting would be beneficial.

The net nonuniformity factor approach developed in this paper offers several advantages over previous closed-form solutions:

- the effects of plasma/slag transverse nonuniformities are automatically included in the model;
- axial leakage currents are implicitly included in the model;
- the number of primary unknowns in the basic model is reduced by two since explicit terms for axial leakage currents and transverse voltage drops are not needed;
- the model corresponds well with channel measurements that realistically can be taken at the CDIF; and
- the model explains many of the trends observed for the CDIF generator during power generation.

Axial nonuniformities and transverse slag leakage effects are generally ignored in this model. However, with the increasing use of iron dopants in the CDIF testing program, axial nonuniformities are becoming much less of a problem. Despite these disadvantages, the model developed in this paper provides a practical tool for analyzing CDIF test data and evaluating the performance of the CDIF generator.

REFERENCES

1. Wu, Y. C. L., "Performance Theory of Diagonal Conducting Wall MHD Generators," AIAA Journal, Vol. 14, October 1976.
2. Nelson, G. L.; Lee, Y. M.; Stepan, I.; Wu, Y. C. L.; and Lineberry, J. T., "Analysis of CDIF Coal-Fired Faraday Generator Test Data," 27th SEAM, Reno, NV, June 1989.
3. Pian, C. C. P.; Petty, S. W.; and McClaine, A. W., "Operating Characteristics of a Slagging Diagonally-Loaded Magnetohydrodynamic Power Generator," 25th SEAM, Bethesda, MD, June 1987.
4. Solbes, A., TRW Interoffice Correspondence MHD-III-87-030, April 1987.
5. Daniel, V. W.; and Lohrasbi, J., "Power-Loss Mechanisms in Coal-Fired MHD Generators," 27th SEAM, Reno, NV, June 1989.
6. Rosa, R. J., Magnetohydrodynamic Energy Conversion, McGraw-Hill Book Company, New York, NY, 1968.
7. Daniel, V. W., "A Simple, One-dimensional, Electrical Model for Linear MHD Generators," MSE Report No. 2DOE-MHD-D157, April 1990.
8. Schiller, D.; Joyce, J.; and Lofftus, D., "MHD Plasma Velocity Measurements using Correlation Techniques," 26th SEAM, Nashville, TN, June 1988.
9. Demetriades, S. T., "Modeling the CDIF MHD Test Train," Report No. STDR-86-17, STD Research Corporation, Monrovia, CA, June 1986.

ACKNOWLEDGEMENT

This work was prepared for the U.S. Department of Energy under contract DE-AC07-88ID12735.